Methacrylate-Based Polymer Foams with Controllable Pore Sizes and Controllable Polydispersities via Foamed Emulsion Templating

Miriam Lucia Dabrowski and Cosima Stubenrauch*

This study reports on a novel templating route, which uses foamed emulsions as templates for porous polymers. The concept is based on the generation of a monomer-in-water emulsion, which is subsequently foamed via microfluidics. The monomer of choice is 1,4-butanediol dimethacrylate (1,4-BDDMA). After polymerization of the foamed emulsion, one obtains open-cell polymer foams with porous pore walls. Foamed emulsions and polymer foams are generated. It is shown that foamed emulsion templating in combination with microfluidics is well-suited to synthesize 1) monodisperse poly(1,4-BBDMA) foams with controllable pore sizes and 2) their polydisperse counterparts with controllable polydispersities. Monodisperse templates with different bubble sizes and thus polymer foams with different pore sizes ranging from about 100–400 μm in diameter are synthesized. Microfluidics is also used for the generation of polydisperse poly(1,4-BDDMA) foams with polydispersities between 18% and 27% but the same mean pore sizes as the monodisperse ones, i.e., we have access to polymer foams that only differ in their polydispersity.

1. Introduction

The synthesis routes of polymer foams are numerous. The most obvious way is the foaming of a precursor solution during polymerization. A well-known example of this method is polyurethane, which is foamed by a blowing agent during the polyaddition of isocyanate and polyol.[1] In recent literature, the synthesis of polymer foams via templating routes have been increasingly focused on. The principle is based on the generation and solidification of a liquid template to control the polymer foam`s morphology. The liquid templates are either high internal phase emulsions (HIPEs) with an internal phase volume of ≥ 74 vol% or foams with liquid fractions, e.g., 0.06–0.11.[2–5] Most HIPEs in literature are water-in-monomer emulsions with the mixture of styrene and divinylbenzene (DVB) being the most prominent example of the continuous phase.[2,5–17] Further hydrophobic monomers that were studied are ethyleneglycol dimethacrylate (EGDMA),[18,19] propylene fumarate (PF) and propylene fumarate diacrylate (PFDA),[20] propylene fumarate dimethacrylate (PFDMA)[19,21–25] and 1,4-butanediol dimethacrylate (1,4-BDDMA).[19,23,26] So far, only a few studies exist where the hydrophilic phase is the continuous phase, namely aqueous solutions of acrylic acid,[27] vinylated gelatin,[28–30] 2-hydroxyethyl methacrylate,[31] alginate,[32] furfuryl alcohol,[33] chitosan,[34,35] or dextranmethacrylate[36] emulsified with toluene,[27–30,32] decane,[33–35] or cyclohexane[31,36] as dispersed phase. There are, however, two far-reaching disadvantages of emulsion templating. First, the pore size is limited by the accessible droplet size. Typically, pore sizes of poly-HIPEs range from 1 to 100 μm.[11] Second, the dispersed phase must be removed after the solidification of the continuous phase. To overcome these problems, foam templates can be used.[5] Here, an aqueous polymer solution is foamed and the polymer is subsequently cross-linked.[4,5] For example, gelatin,[37,38] polyvinylalcohol,[39] and polysaccharides such as alginates,[40–43] hyaluronic acid,[41] or chitosan[3,4,41,44–46] were used. However, the solubility of hydrophilic polymers in water is limited and typically ranges between 4% and 15%.[3,4]

Is there a way to combine foam templating with a large amount of polymer or monomer in the continuous phase? Yes! One can either increase the solubility of the polymer via a chemical modification as shown for gelatin in refs. [47–49] or one can emulsify a hydrophobic monomer and foam the resulting monomer-in-water emulsion.[14,50–54] Salonen et al. studied the foaming of oil-in-water (o/w) emulsions, so-called foamed emulsions or "foamulsions". However, they used nonpolymerisable oils.[55] Schüler et al. studied the foaming and

M. L. Dabrowski, Prof. C. Stubenrauch
Institute of Physical Chemistry
University of Stuttgart
Pfaffenwaldring 55, 70569 Stuttgart, Germany
E-mail: Cosima.Stubenrauch@ipc.uni-stuttgart.de

Prof. C. Stubenrauch
Institute of Advanced Studies (USIAS)
Université de Strasbourg
F-67000, France

The ORCID identification number(s) for the author(s) of this article can be found under https://doi.org/10.1002/adem.202001013.

polymerization of styrene-in-water emulsions as a complementary templating route.[50] The continuous phase consisted of 65 vol% styrene and the bubble size ranged from ≈20 to ≈100 μm resulting in polydisperse polystyrene foams with pore sizes ranging from around 20 to 200 μm. In follow-up studies of the same system, it was shown that the bubble size can be as large as 588 μm and that monodisperse polystyrene foams can be synthesized.[14,51–53] Moreover, polymer foams synthesized via foamed emulsion templating have a "sub-porosity" in the pore walls which is obtained after water is removed.[50–52,54] Note that only five studies exist about the polymerization of foamed emulsions, all of which deal with the monomer styrene.

A quickly increasing number of studies deals with biodegradable polymer foams for tissue engineering where the polymer foams are supposed to act as scaffolds which facilitate tissue regeneration.[21–25,28–30,32,36–43,56–58] Biodegradable and biocompatible polymer foams are suitable as scaffolds if they have a 3D and highly porous structure with interconnected pores ranging from 50 to 500 μm.[5,56–58] Note that the interconnection of the pores is fundamental for the supply of nutrients.[36,39,42,43,58] Recent findings suggest that a homogeneous, monodisperse pore structure is advantageous for cell seeding and cell growth by ensuring uniform transport of nutrients and uniform degradation of the scaffold.[39,43] Mechanically stable materials are obtained with PF[20] or PFDMA[19,21–25] and can be used as scaffolds in hard tissue engineering for the regeneration of bones. So far, most scaffolds synthesized via emulsion or foam templating are based on hydrophilic polymers such as collagen or chitosan.[28–30,36–43] Moglia et al. and Robinson et al. were the first who synthesized hydrophobic methacrylate-based polymer foams via emulsion templating as scaffolds for bone tissue engineering.[19,21–23] To the best of our knowledge, only polydisperse PFDMA- and 1,4-BDDMA-based polymer foams do exist. Inspired by these studies, we used 1,4-BDDMA for the synthesis of monodisperse polymer foams via emulsion templating using microfluidics with pore diameters ranging from around 70 to 120 μm.[26] For the synthesis of poly(1,4-BDDMA) foams with even larger pore diameters of 200 and 400 μm, we used foamed emulsion templating. Given by the nature of this special templating route, only open-cell polymer foams with interconnected pores are obtained. In our previous study, we focused on finding a composition of the 1,4-BDDMA-in-water emulsion that meets all requirements as regards foam stability and foamability.[54] In the present study, we foamed this emulsion using microfluidics and subsequently polymerized the template (**Scheme 1**). We synthesized monodisperse poly(1,4-BDDMA) foams with pore sizes ranging from 100 to 400 μm and polydisperse poly(1,4-BDDMA) foams with polydispersities between 18% and 27% but the same average pore sizes as the monodisperse counterparts. We emphasize that this is the first study about the synthesis of methacrylate-based polymer foams with controllable structure via foamed emulsions. The challenges one has to deal with are threefold. First, one has to find a proper formulation for the foamed emulsion, which is not straightforward considering the lack of knowledge in this new field. Second, one has to generate the liquid template with the desired structure. Third, one has to find the proper polymerization conditions such that the structure of the template is retained during solidification.
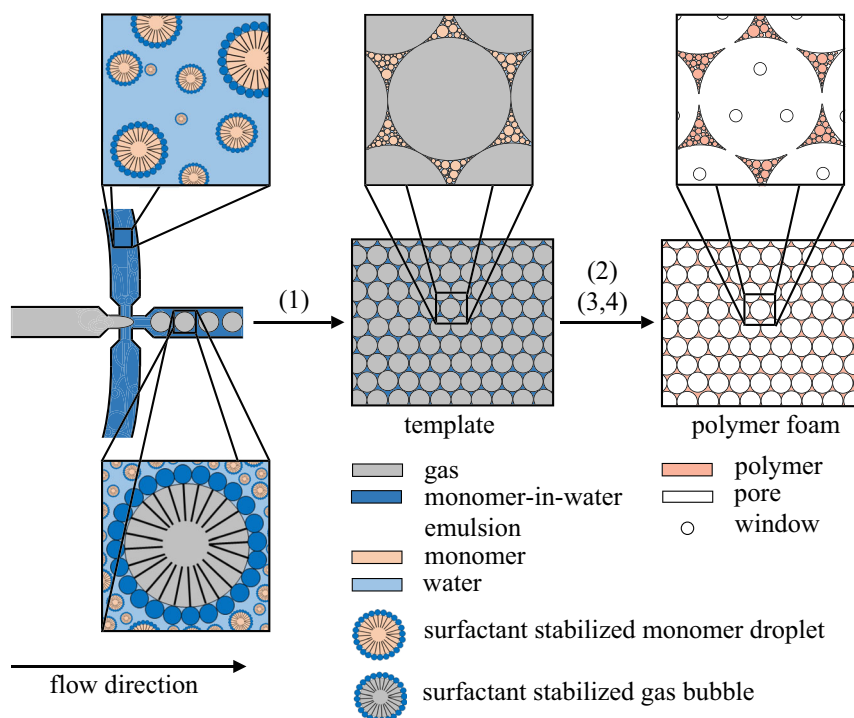
Scheme 1. Concept of the synthesis of polymer foams using foamed emulsions as templates. (1) Generation of the monodisperse foamed monomer-in-water emulsion template via microfluidics, (2) polymerization of the monomer, (3,4) purification of the polymer foam followed by its drying.

2. Results and Discussion

2.1. Calibration of Microfluidic Chips

To determine the range of synthesizable pore sizes, it is necessary to first analyze the variety of bubble sizes which can be generated by calibrating the microfluidic system. The continuous phase consists of the monomer-in-water emulsion, while N_2 was the dispersed phase (Section Polymer Foam Synthesis). We used three microfluidic chips called: (100×105) μm chip, (190×195) μm chip, and (275×280) μm chip (for details, see Section Microfluidic Device). During calibration of one microfluidic chip, the continuous phase pressure was kept constant, whereas the dispersed phase pressure was varied (see Section Microfluidic Device). The smallest possible bubble diameter with the respective microfluidic chip can be obtained using the smallest available pressure settings for the dispersed phase. A stepwise increase in the dispersed phase pressure led to monodisperse bubbles of increasing sizes, with the largest bubble diameter being generated by applying the highest available pressure. The diameter of both the smallest and the largest bubbles depend on the microfluidic chip constriction. Inside each microfluidic chip, three things happen. First, the bubbles arrange in a single-row flow. Second, the bubbles sizes increase with increasing pressure of the dispersed phase. Third, the bubbles are packed more tightly and deform more and more from spheres to ellipsoids as the dispersed phase pressure increases.

For the calibration of the chips, all monodisperse bubble diameters with a polydispersity index (PDI) of ≤5% were plotted against the pressure of the dispersed phase (**Figure 1**). Note that each calibration curve is highly correlated to the conditions presented during the calibration, which is the reason why a calibration may not be completely reproducible. Thus, a calibration curve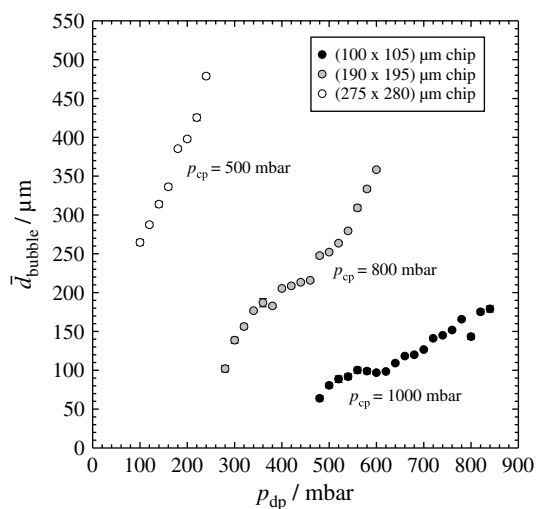 of a microfluidic system can only be regarded as a guideline outlining the generable bubble sizes and the needed pressure settings. As mentioned earlier and as can be seen in Figure 1, an increase in the dispersed phase pressure leads to an increase in the mean bubble diameter for all microfluidic systems. The standard deviation of each mean bubble diameter reflects the general sensitivity of the experimental procedure and during the quantitative characterization of the bubbles sizes. Using the (100×105) μm chip, mean bubble diameters ranging from 64 μm ± 3 μm (PDI = 5%) to 179 μm ± 4 μm (PDI = 2%) were obtained. Using the (190×195) μm chip, mean bubble diameters ranging from 102 μm ± 4 μm (PDI = 4%) to 358 μm ± 2 μm (PDI = 1%) were obtained. Using the (275×280) μm chip, mean bubble diameters ranging from 264 μm ± 4 μm (PDI = 1%) to 479 μm ± 3 μm (PDI = 1%) were obtained. To sum up, we are able to generate bubbles in a range from 60 to 480 μm.

2.2. Monodisperse Poly(1,4-BDDMA) Foams via Foamed Emulsion Templating

2.2.1. Monodisperse Foamed Emulsion Templates

The first aim of this study was to synthesize monodisperse 1,4-BDDMA-based polymer foams with increasing pore sizes via foamed emulsion templating. Hence, we formulated and foamed 1,4-BDDMA-in-water emulsions. The left-hand side of **Figure 2** shows the microscope pictures of the three monodisperse foamed emulsion monolayers, while the right-hand side shows the corresponding bubble size distributions.

As shown in Figure 2, we obtained foamed emulsion templates with increasing mean bubble diameters (top left to bottom left) from 99 μm ± 1 μm (PDI = 1%), 199 μm ± 2 μm (PDI = 1%), and 399 μm ± 5 μm (PDI = 1%). The microscope pictures and the bubble size distributions extracted hereof (**Table 1**) reveal that the foamed emulsion templates are monodisperse (PDI ≤ 5%).[59,60]

2.2.2. Monodisperse Poly(1,4-BDDMA) Foams

The three monodisperse foamed emulsion templates in Figure 2 (Section 2.2.1) were subsequently polymerized (see Section Polymer Foam Synthesis) and characterized (see Section Optical Microscopy and Determination of Bubble Diameters). Note that in Figure 2, monolayers of the foamed emulsions are shown as they are easier to characterize. The samples that were finally polymerized consisted of a couple of layers of densely packed monodisperse gas bubbles as in all our previous studies. Thus, the gas content of all monodisperse templates was 74 vol% as explained in ref. [59]. The left-hand side of **Figure 3** shows the scanning electron microscope (SEM) pictures of the three monodisperse poly(1,4-BDDMA) foams, whereas the right-hand side shows the corresponding pore size distributions. The mean pore diameters, the PDIs and the mean window diameters are listed in Table 1. Looking at Figure 3 and Table 1, one sees four trends: 1) The mean bubble and mean pore diameters are nearly the same. 2) The PDIs of the polymer foams are slightly higher than those of the liquid templates, which is in line with our previous studies (see, e.g., refs. [3,14,26,45,52,54]). The PDIs change due to

Figure 1. Mean bubble diameter $\overline{d}_{bubble}$ as a function of the pressure of the dispersed phase p_{dp} for three microfluidic chips having constrictions of (100×105) μm, (190×195) μm, and (275×280) μm. The continuous phase pressure p_{cp} was kept constant at 1000 mbar $((100 \times 105)$ μm), 800 mbar (190×195) μm (left), and 500 mbar (275×280) μm (right), while the dispersed phase pressure was varied in 20 mbar steps.

**ADVANCED
SCIENCE NEWS**

www.advancedsciencenews.com

*ADVANCED
ENGINEERING
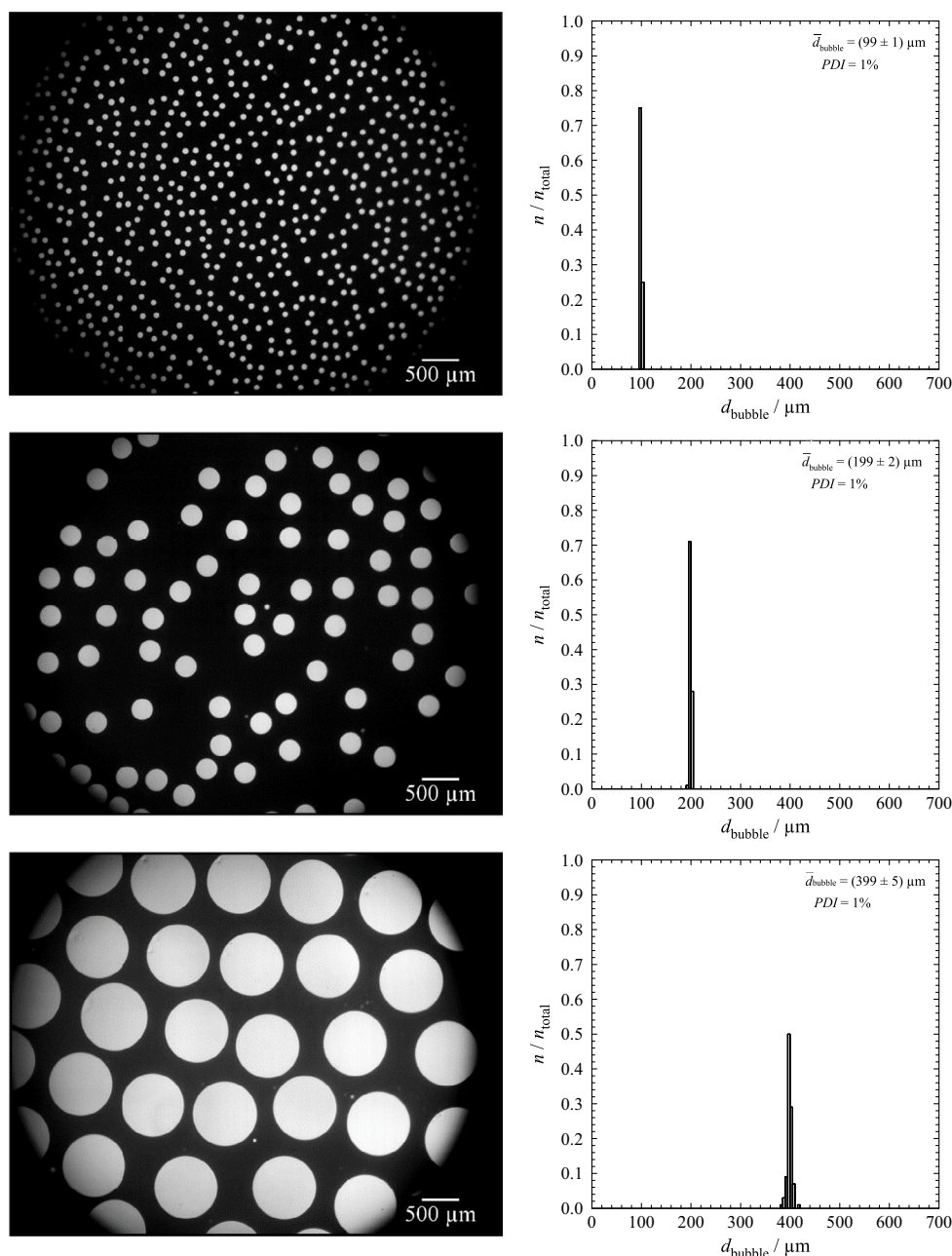MATERIALS*

www.aem-journal.com

Figure 2. Microscope pictures of monolayers of monodisperse 1,4-BDDMA-based foamed emulsion templates with bubble diameters of around 100 μm using the (100 × 105) μm chip (top left), 200 μm using the (190 × 195) μm chip (middle left), and 400 μm using the (275 × 280) μm chip (bottom left) and the corresponding bubble size distributions with $n_{total} = 100$ (right).

an unavoidable disintegration of the foamed emulsion during polymerization. However, the very similar mean bubble and mean pore diameters show that a disintegration takes place to a minor extent only. 3) The mean pore and the mean window diameters increase in the same relative way, which is also in line with a previous study.[61] 4) As shown in **Figure 4**, using higher magnifications, the pore walls have a "sub-porosity", as was also demonstrated in ref. [50–52,54]. The porosity stems from the fact that the continuous phase of the liquid template (monomer-in-water emulsion) partly consists of water,

which causes the porosity in the pore walls after polymerizing and drying.

2.3. Polydisperse Poly(1,4-BDDMA) Foams via Foamed Emulsion Templating

2.3.1. Polydisperse Foamed Emulsion Templates

Polydisperse polymer foams synthesized via foamed emulsion templating exist for polystyrene[50] and poly(1,4-BDDMA).[26]

2001013 (4 of 12)

Table 1. Mean bubble diameters $\bar{d}_{bubble}$ and PDIs of monodisperse monolayers of the foamed emulsion templates as well as mean pore diameters $\bar{d}_{pore}$, PDIs, and mean window diameters $\bar{d}_{window}$ of the monodisperse poly(1,4-BDDMA) foams.

Monodisperse foamed emulsion template		Monodisperse polymer foam		
$\bar{d}_{bubble}$ [µm]	PDI [%]	$\bar{d}_{pore}$ [µm]	PDI [%]	$\bar{d}_{window}$ [µm]
99 ± 1	1	107 ± 15	14	21 ± 7
199 ± 2	1	196 ± 8	4	44 ± 6
399 ± 5	1	389 ± 31	8	107 ± 27

However, in these two studies, the templates were generated via mechanical mixing, i.e., a precise control of the bubble size and the bubble size distribution was not possible. If one wants to study the influence of the polydispersity on the polymer foam properties, one needs to be able to control the bubble size of the template and to adjust the polydispersity. This, in turn, is possible with microfluidics. The procedure for the synthesis of polymer foams with controllable polydispersity was developed by Andrieux et al.[3] using chitosan-based liquid foams and successfully transferred to 1,4-BDDMA-based emulsions by us.[26] Irrespective of the kind of template used, the resulting polydispersity of the template and of the polymer foam depends
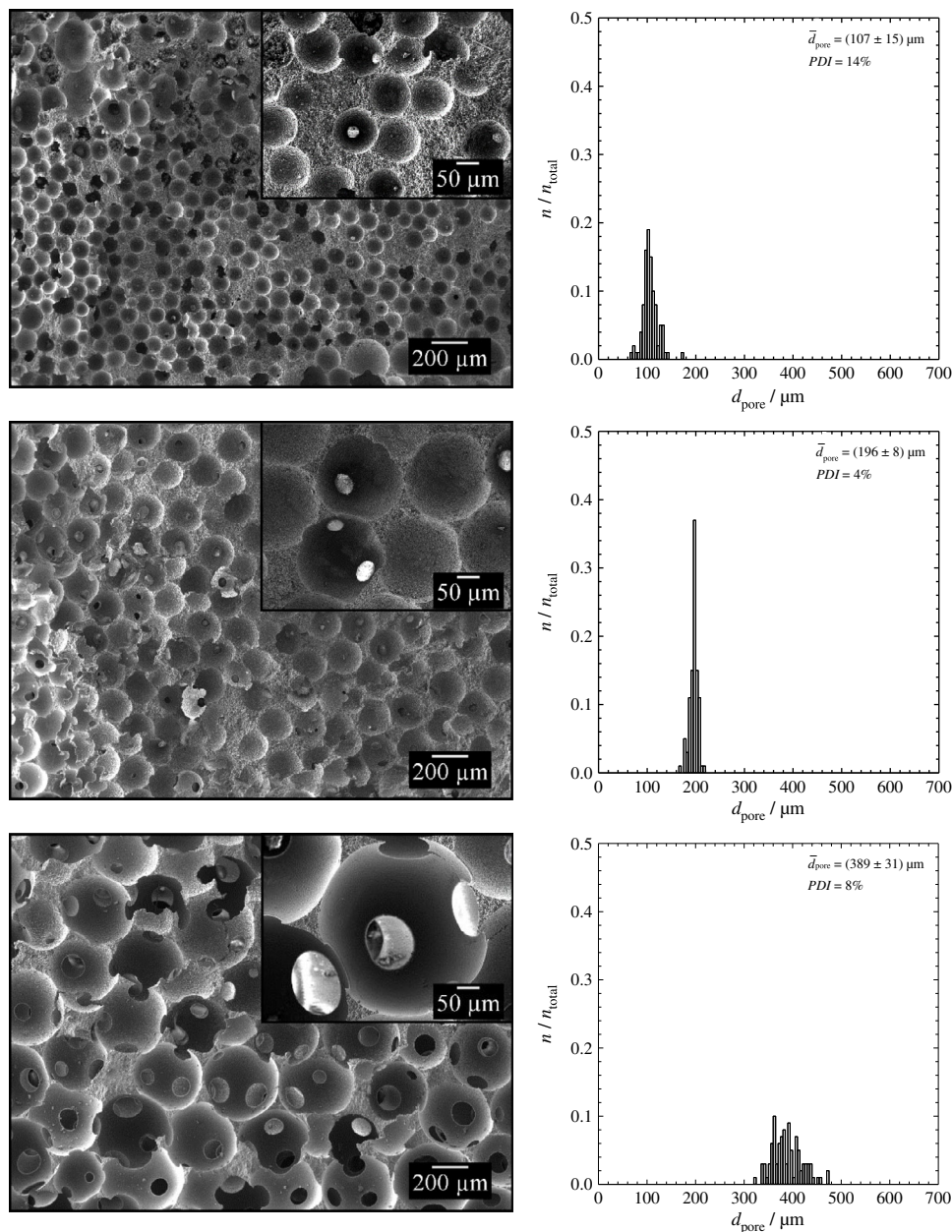

Figure 3. SEM pictures of specimens of monodisperse poly(1,4-BDDMA) foams synthesized via foamed emulsion templating with pore diameters of around 100 µm (top left), 200 µm (middle left), 400 µm (bottom left) and the corresponding pore size distributions with $n_{total} = 100$ (right).
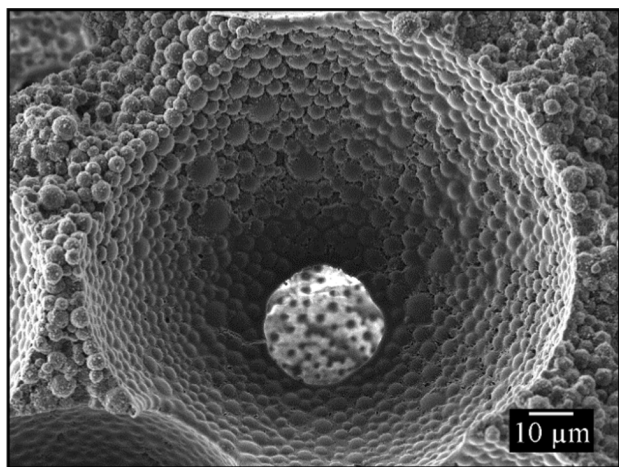
Figure 4. Close-up SEM picture of the fine structure of a specimen of a poly(1,4-BDDMA) foam having a pore size of 107 μm ± 15 μm.

on 1) the microfluidic chip constriction (the larger the constriction, the larger are the bubbles/pores and the lower is the PDI), 2) the absolute values of the pressure amplitudes which define the smallest and the largest bubble/pore sizes (the larger the amplitude, the higher is the PDI), and 3) the period between two equal amplitudes which defines the number of repetition (the larger the period, the smaller is the PDI). The second aim of this study was to synthesize polydisperse poly(1,4-BDDMA) foams with a controllable polydispersity of around 25% but the same mean pore diameters, i.e., poly(1,4-BDDMA) foams of 100 μm ± 25 μm, 200 μm ± 50 μm, and 400 μm ± 100 μm were aimed for. The polymer foams were synthesized as described in Section Polymer Foam Synthesis and characterized as described in Section Optical Microscopy and Determination of Bubble Diameters. The left-hand side of **Figure 5** shows the microscope pictures of the three polydisperse foamed emulsion monolayers, whereas the right-hand side shows the corresponding bubble size distributions.

The microscope pictures in Figure 5 show polydisperse foamed emulsion templates of increasing bubble sizes from 108 μm ± 26 μm and a PDI of 24%, 231 μm ± 40 μm and a PDI of 17%, and 414 μm ± 73 μm and a PDI of 18%. The microscope pictures, the calculated data (also given in **Table 2**), and the bubble size distributions reveal that the polydispersites of the foamed emulsions are indeed very similar, i.e., are indeed controllable.

2.3.2. Polydisperse Poly(1,4-BDDMA) Foam

After the generation of the polydisperse foamed emulsion templates (see Section 2.3.1, Figure 5), the templates were polymerized to synthesize polydisperse poly(1,4-BDDMA) foams. As was the case for the monodisperse counterparts, the samples that were polymerized consisted of a couple of layers densely packed gas bubbles. As the polydispersity we deliberately added to the system is not very high, the gas content of all samples is between 64 and 74 vol% as explained in ref. [59]. The left-hand side of **Figure 6** shows the SEM pictures of the three polydisperse

poly(1,4-BDDMA) foams, whereas the right-hand side shows the corresponding pore size distributions. The mean pore diameters, the PDIs and the mean window diameters are listed in Table 2. Figure 6 and Table 2 reveal again four trends: 1) The mean bubble diameters are slightly smaller than the mean pore diameters. 2) The PDIs of the polymer foams are very similar to the PDIs of the foamed emulsion templates, which is in line with our previous study on poly(1,4-BDDMA) foams with a controllable polydispersity.[26] 3) The mean pore and the mean window diameters increase in the same relative way. 4) There is a "sub-porosity" in the pore walls, which means that the pore walls are also porous as also reported in ref. [50–52,54]. Due to the fact that the polymer matrix is always the same, we did not show an additional SEM picture of the fine structure of polydisperse polymer foams as it is the same as the one seen in Figure 4. In comparison to the monodisperse poly(1,4-BDDMA) foams, much larger window sizes were obtained. In general, the fact that it is possible to synthesize polymer foams with a controllable polydispersity, but the same mean pore size as their monodisperse counterparts is useful for many applications and for testing the impact of the polydispersity on the mechanical properties of the polymer foam.

2.4. Mechanical Properties

We measured stress–strain curves of a monodisperse polymer foam and its polydisperse counterpart (three samples in each case). As shown in **Figure 7**, the curves nearly lie on top of each other. A look at **Table 3** reveals that the densities of the two samples are also very similar. Note that the density of the polydisperse polymer foam is slightly lower which is reflected in a slightly lower modul E_{foam} (see values in Table 3). These findings are in line with what one expects: The mechanical properties of porous solids, i.e., of solid foams, have been widely investigated and there is a general agreement that the relative Young's modulus ($E_{foam}/E_{polymer}$) as well as the relative shear modulus ($G_{foam}/E_{polymer}$) directly depend on the squared relative density ($\rho_{foam}/\rho_{polymer}$)^2. Here, we will discuss the relative Young's modulus only for which it holds

$$\frac{E_{foam}}{E_{polymer}} = C_c \left(\frac{\rho_{foam}}{\rho_{polymer}} \right)^2 \tag{1}$$

with $C_c \approx 1$ according to Gibson and Ashby.[62–64] Looking at Table 3, one sees that the relative Young's modulus ($E_{foam}/E_{polymer}$) of our polymer foams indeed is proportional to ($\rho_{foam}/\rho_{polymer}$)^2 with a proportionality factor of ≈ 1 in case of the monodisperse foams and of ≈ 1.7 in case of the polydisperse foam, which is in the usual range. We conclude that the mechanical properties solely depend on the polymer foam's density and not on its polydispersity. Calculating the porosities from the densities (see Section (SEM); Determination of Pore and Window Diameters), one sees that the porosities are in the range of 85–90% and not $\approx 74\%$ as expected for a densely packed system of monodisperse pores. The reason for this difference was already described qualitatively in Section 2.2. and Section 2.3.2, namely the "sub-porosity" in the pore walls.
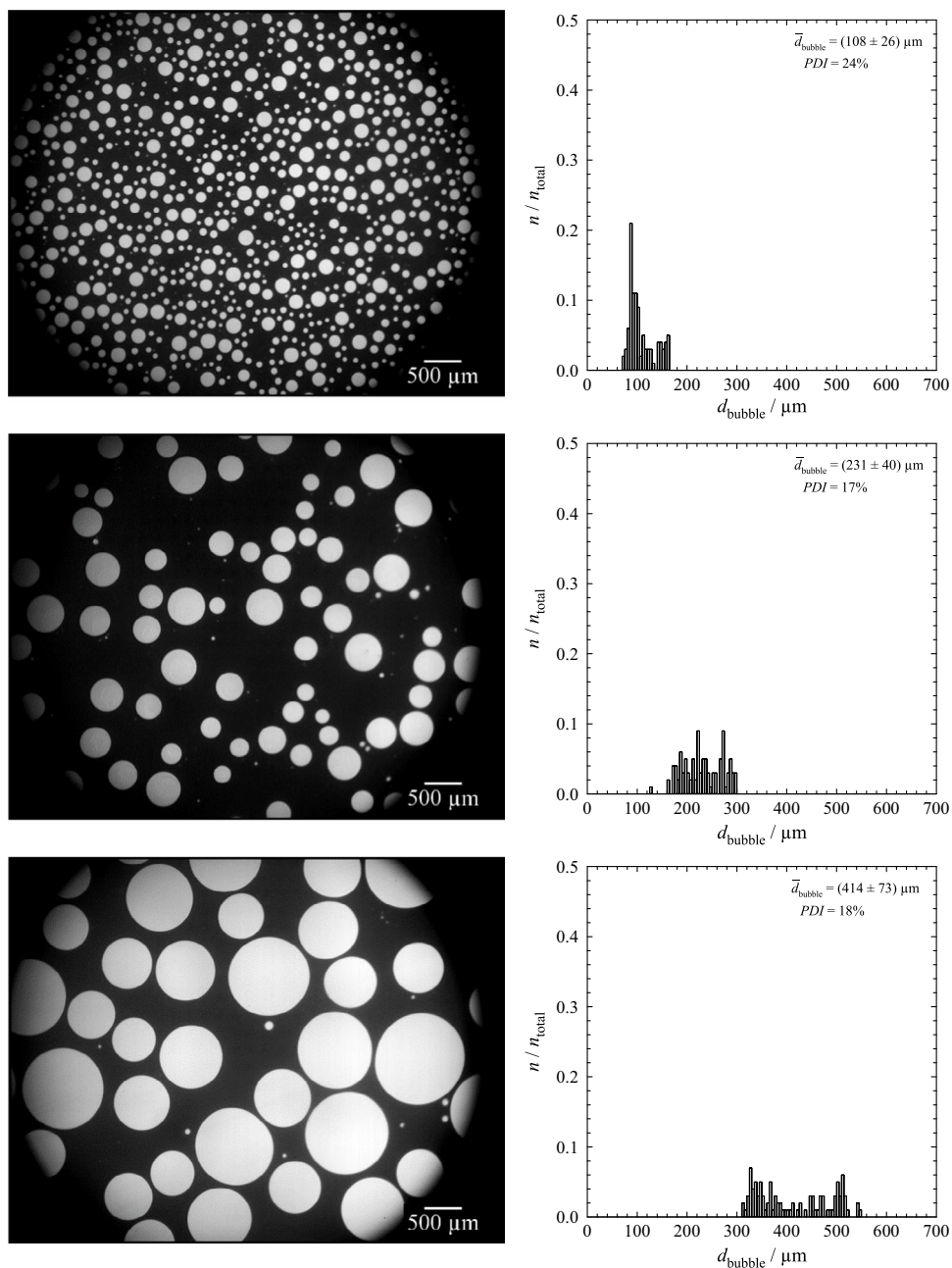
Figure 5. Microscope pictures of monolayers of polydisperse 1,4-BDDMA-based foamed emulsion templates with bubble diameters of around 100 µm ± 25% using the (100 × 105) µm chip (top left), 200 µm ± 25% using the (190 × 195) µm chip (middle left), and 400 µm ± 25% using the (275 × 280) µm chip (bottom left) and the corresponding bubble size distributions with $n_{total} = 100$ (right).

3. Conclusion and Outlook

In this study, we synthesized and characterized methacrylate-based open-pore polymer foams using a novel templating route, called foamed emulsion templating. For this purpose, we used the hydrophobic monomer 1,4-BDDMA to formulate, foam, and polymerize a 1,4-BDDMA-in-water emulsion. Microfluidics was used as foaming method. Three microfluidic chips were used to generate foamed emulsion templates of different sizes. Three monodisperse poly(1,4-BDDMA) foams with mean pore diameters ranging from around 100–400 µm were synthesized, and these polymer foams had the desired structure: monodisperse, highly porous, closed-packed, open-pore. We also synthesized three polydisperse poly(1,4-BDDMA) foams with polydispersities between 18% and 27% but the same mean pore diameters as their monodisperse counterparts and obtained porous and closed-packed structures of highly interconnected pores. In both cases (mono- and polydisperse), the increase in the pore sizes is accompanied by an increase in the window sizes. The main findings are: 1) Foamed emulsion templating is

Table 2. Mean bubble diameters $\bar{d}_{bubble}$ and PDIs of the polydisperse monolayers of the foamed emulsion templates as wells as mean pore diameters $\bar{d}_{pore}$, PDIs, and mean window diameters $\bar{d}_{window}$ of the polydisperse poly(1,4-BDDMA) foams.

Polydisperse foamed emulsion template		Polydisperse polymer foam		
$\bar{d}_{bubble}$ [µm]	PDI [%]	$\bar{d}_{pore}$ [µm]	PDI [%]	$\bar{d}_{window}$ [µm]
108 ± 26	24	133 ± 32	24	34 ± 8
231 ± 40	17	240 ± 44	18	68 ± 18
414 ± 73	18	444 ± 121	27	159 ± 78

well-suited to synthesize monodisperse poly(1,4-BBDMA) foams with controllable pore size and their polydisperse counterparts with controllable polydispersities. 2) The window sizes increase with increasing pore sizes. 3) Beyond to the large pores, a "sub-porosity" is created in the pore walls caused by the nature of the continuous phase, i.e., the evaporation of water. 4) The pore sizes accessible via foamed emulsion templating are much larger than those of emulsion templated poly(1,4-BBDMA) foams. These four findings make foamed emulsion templating very interesting for various areas of applications, e.g., tissue engineering. Providing an additional porosity within the pore walls may speed up the biochemical supply throughout the scaffold,
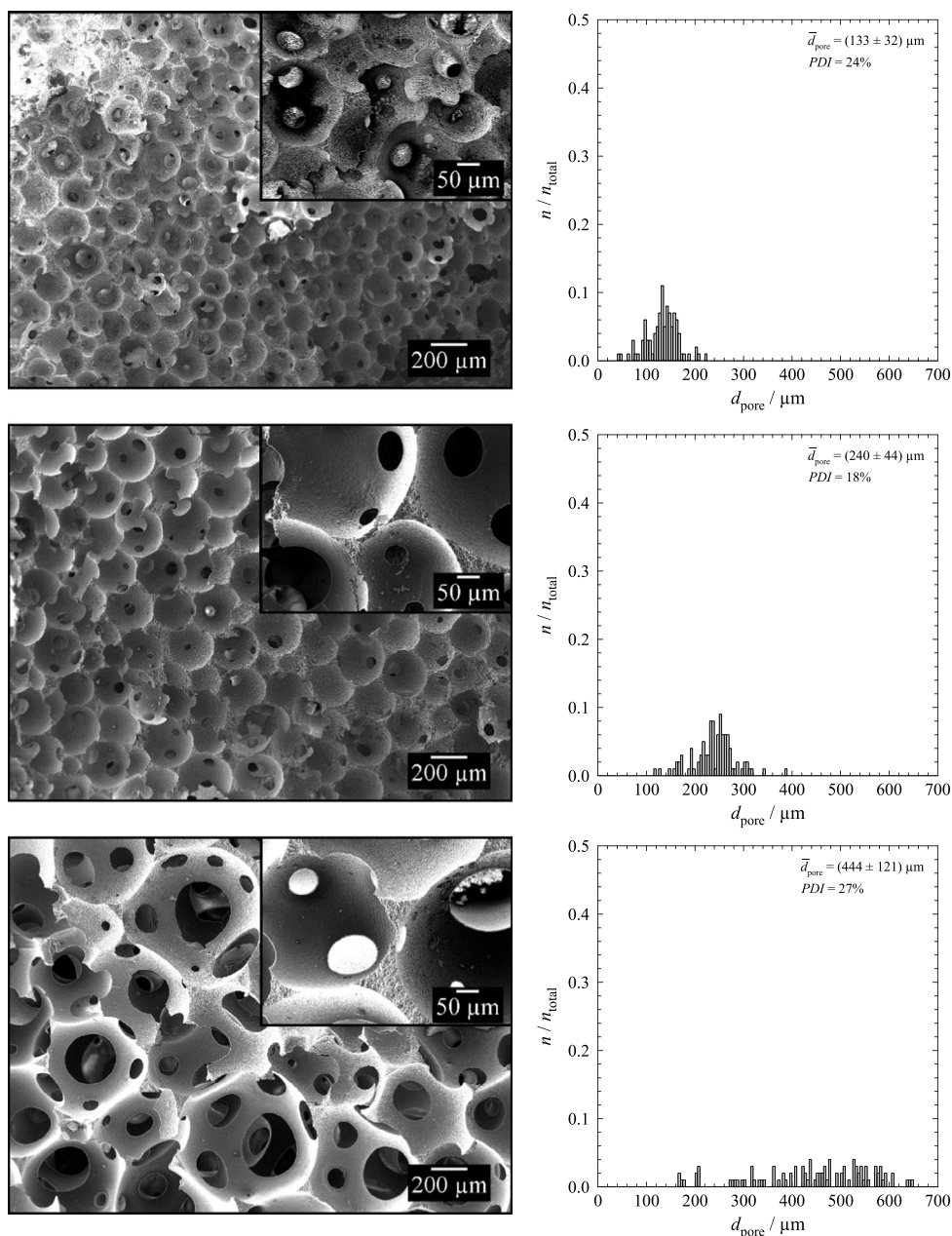

Figure 6. SEM pictures of specimens of polydisperse poly(1,4-BDDMA) foams synthesized via foamed emulsion templating with pore diameters of around 100 µm ± 25% (top left), 200 µm ± 25% (middle left), 400 µm ± 25% (bottom left) and the corresponding pore size distributions with $n_{total} = 100$ (right).

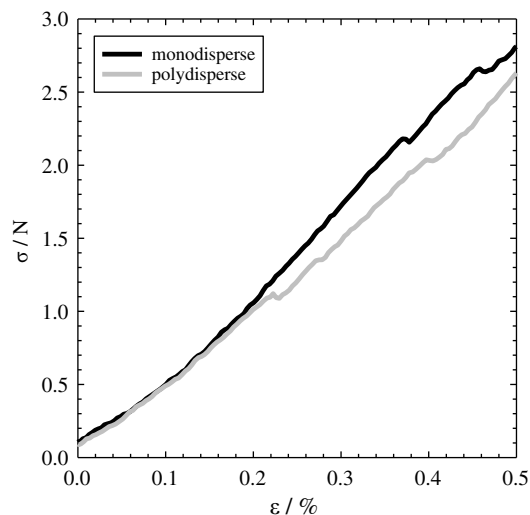**Figure 7.** Stress (σ)–strain (ε) curve of one monodisperse and one polydisperse poly(1,4-BDDMA) foam having a pore size of $\approx 400\,\mu m$.

thus facilitating the growth of tissue. Furthermore, foaming emulsions via microfluidics allows to adjust the polydispersity, which is necessary for two reasons. So far, it is still unclear 1) which polydispersity is needed for scaffolds in tissue engineering and 2) how the polydispersity influences the polymer foam's mechanical properties. Consequently, the aim of our future study is to measure the densities and the mechanical strength of our polymer foams. As biodegradable polymers are needed for tissue engineering, follow-up studies will deal with PFDMA-based polymer foams, with the study at hand serving as scouting system.

4. Experimental Section

Materials: 1,4-BDDMA 95% containing 200–300 ppm hydroquinone monomethylether (MeHQ) as inhibitor, sodium dodecyl sulfate (SDS, ≥99%), benzoylperoxide (BPO, Luperox A75, 75%) and glycerol were purchased from Sigma Aldrich. Bi-distilled water (further called water) was used. Ethanol was used for Soxhlet extraction. All chemicals were used as received and not further purified.

Polymer Foam Synthesis: The synthesis of monodisperse and polydisperse poly(1,4-BDDMA) foams via foamed emulsion templating consists of five steps: 1) The preparation of the continuous phase, i.e., the polydisperse 1,4-BDDMA-in-water emulsion ($V_{emulsion} = 20\,mL$), 2) its homogenization, 3) the foaming of the emulsion via microfluidics, and 4) the subsequent polymerization of the monomer droplets. Step (5) includes the purification and drying of the synthesized poly(1,4BDDMA) foams. 1) For the preparation of the emulsion 65 vol% 1,4-BDDMA (13.30 g; 0.0588 mol), 30 vol% water (6 g), 5 vol% glycerol (1.26 g), and 5 wt% SDS (1.03 g) were stepwise added and mixed with a magnetic stirrer

(30 min, 1000 rpm). Then, 2 mol% of the initiator BPO (calculated with respect to the amount (mol) of the monomer 1,4-BDDMA; 0.28 g) was added; the emulsion was placed in an ice bath and mixed with a magnetic stirrer (25 min, 1000 rpm). The emulsion needs to be cooled to prevent the decay of initiator due to heat dissipation during the subsequent homogenization. 2) The further cooled emulsion was homogenized three times (each time for 40 s) at a power of 30% using an ultrasonic homogenizer SONOPULS HD2200 from Bandelin to decrease the 1,4-BDDMA droplet sizes which, in turn, increases the stability of the emulsion. 3) The foaming of the 1,4-BDDMA-in-water emulsion was carried out via microfluidics (Section Microfluidic Device). The foamed emulsion template was collected in a glass tube (VWR, 4 mL, 44.6 mm × 14.65 mm, $\varnothing_{inner} \approx 1.3\,cm$) up to a height of 4 cm, sealed, and 4) subsequently polymerized via UV-polymerization for 4 h by placing the foamed emulsion templates in the middle between two MH-Modul 250W Z4 XL (à 250 W) UV lamps from Hereaus with a radiation in a spectral range between 250 and 550 nm. The distance between the two UV lamps was 60 cm to prevent a heating of the foamed emulsions. 5) After breaking the glass tube (necessary to obtain the polymer foam), Soxhlet extraction was carried out with ethanol at 100 °C to purify the polymer foams from residual emulsion components or initiator. All polymer foams were purified for at least 12 h and dried for 72 h at room temperature.

Microfluidic Device: Microfluidics was used to foam the 1,4-BDDMA-in-water emulsions (i.e., the continuous phase) with nitrogen (i.e., the dispersed phase). The continuous phase was prepared as described in Section Polymer Foam Synthesis. Different bubble sizes were obtained using the flow-focusing chip geometry (X-Junction) of three different hydrophilic microfluidic glass chips purchased from Dolomite with the dimensions listed in **Table 4**.

After formulation, the continuous phase was placed in a 100 mL glass bottle (Schott), while a second 100 mL glass bottle remained empty. Both glass bottles were sealed with Vaplock GL45 caps. Each glass bottle was connected to the pressure controller Elveflow OB1 MKIII+ and with FEP tubings (Dolomite, $\varnothing_{outer} = 1.6\,mm$, $\varnothing_{inner} = 0.5\,mm$) to the chip. Nitrogen, regulated by the software of the pressure controller Elveflow Smart Interface (Elveflow), was used 1) to push the emulsion with a constant pressure through the two outer inlet channels of the chip and 2) as dispersed phase in the foamed emulsion (pushed through the inner inlet channel of the chip). Depending on the chip, one pressure value of the continuous phase was defined and kept constant (**Table 5**). To generate monodisperse foamed emulsion templates, the pressure value used for pushing the dispersed phase was kept constant. To generate polydisperse foamed emulsion templates, the pressure values changed periodically (amplitude = ±25%) over a period of $\tau = 10\,s$ around the pressure value used for the monodisperse foamed emulsions. Table 5 gives an overview about the used pressure settings.

Table 4. Microfluidic chip specifications.[66]

Microfluidic chip	Constriction		Channels	
	Depth [μm]	Width [μm]	Depth [μm]	Width [μm]
(100 × 105) μm	100	105	100	300
(190 × 195) μm	190	195	190	390
(270 × 275) μm	275	280	275	475

Table 3. Mean density $\overline{\rho}_{foam}$, mean relative density $\overline{\rho}_{foam}/\overline{\rho}_{polymer}$, mean Young's modulus $\overline{E}_{foam}$, and normalized young's modulus $\overline{E}_{foam}/\overline{E}_{polymer}$ for monodispere and polydisperse poly(1,4-BDDMA) foams having a pore size of $\approx 400\,\mu m$. The mean density of 1,4-BDDMA is $\overline{\rho}_{polymer} = (1118 \pm 33)\,kg\,m^{-3}$ and the mean Young's modulus is $\overline{E}_{polymer} = (275 \pm 23)\,MPa$.

Monodisperse				Polydisperse			
$\overline{\rho}_{foam}$ [kg m^{-3}]	$\frac{\overline{\rho}_{foam}}{\overline{\rho}_{polymer}}$	$\overline{E}_{polymer}$ [MPa]	$\frac{\overline{E}_{foam}}{\overline{E}_{polymer}}$	$\overline{\rho}_{foam}$ [kg m^{-3}]	$\frac{\overline{\rho}_{foam}}{\overline{\rho}_{polymer}}$	$\overline{E}_{polymer}$ [MPa]	$\frac{\overline{E}_{foam}}{\overline{E}_{polymer}}$
140 ± 12	0.13 ± 0.01	5.3 ± 1.1	0.019 ± 0.004	115 ± 11	0.10 ± 0.01	4.7 ± 0.2	0.017 ± 0.001

Table 5. Pressure settings of the continuous phase p_{cp} and dispersed phase p_{dp} used for the generation of monodisperse and polydisperse foamed emulsions with three different microfluidic chips and the corresponding mean bubble diameters.

Microfluidic chip	Monodisperse foamed emulsions			Polydisperse foamed emulsions		
	$\bar{d}_{bubble}$ [µm]	p_{cp} [mbar]	p_{dp} [mbar]	$\bar{d}_{bubble}$ [µm]	p_{cp} [mbar]	p_{dp} [mbar]
(100×105) µm	99 ± 1	1000	650	108 ± 26	1000	570–720
(190×195) µm	199 ± 2	800	400	231 ± 40	800	320–480
(270×275) µm	399 ± 5	500	210	414 ± 73	500	160–260

The generation of monodisperse and polydisperse bubbles were observed with the optical microscope Nikon SMZ745T equipped with the high-speed camera Mikroton EoSens CL MC1362, while microscope pictures of the bubble generation and foamed emulsion monolayers were taken using the corresponding software MotionBLITZ Director2 Kit from Mikroton. A Schott KL 1500 compact (150 W) combined with a Mitos microscope stage (Dolomite) by an optical fiber served as light source. Irrespective of the template's polydispersity, the final foamed emulsion template was collected in a glass tube after leaving the outlet channel of the microfluidic chip and transported through a tubing. In case of the (100×105) µm and (190×195) µm microfluidic chips, the dimensions of the outlet tubing corresponds to the dimensions of the inlet tubings (Dolomite, $\varnothing_{outer} = 1.6$ mm, $\varnothing_{inner} = 0.5$ mm), whereas in case of the (270×275) µm microfluidic chip, an outlet tubing of the same material having a larger inner diameter was used (Techlab, FEP tubing, $\varnothing_{outer} = 1.6$ mm, $\varnothing_{inner} = 0.8$ mm), whereas the inlet tubings were not changed.

Calibration: The microfluidic set-up containing the respective chip was calibrated initially to the template generation. The continuous phase pressure was kept constant at 1000 mbar ((100×105) µm chip), 800 mbar ((190×195) µm chip), and 500 mbar ((275×280) µm chip). The dispersed phase pressure was varied in 20 mbar steps from 480 mbar to 840 mbar ((100×105) µm chip), from 280 and to 600 mbar ((190×195) µm chip), and from 100 mbar and to 240 mbar ((275×280) µm chip). At each pair of pressure settings, a foamed emulsion monolayer was created and microscope pictures were taken (Section Calibration).

Optical Microscopy and Determination of Bubble Diameters: Foamed emulsions (generated as described in Section Polymer Foam Synthesis and Microfluidic Device) were characterized using the optical equipment mentioned in Section Microfluidic Device. For preparing the foamed emulsion monolayers, we used the procedure described in ref. [51]. The foamed emulsion was collected on a microscope glass slide (76 mm × 52 mm × 1 mm) which held two adhesive strips of a thickness of 55 µm (Tesafilm, customer service) lengthwise at its shorter ends. For calibration means, one foamed emulsion droplet or a part of it was collected. In case of monodisperse foamed emulsion templates, one droplet was collected. In case of polydisperse foamed emulsion templates, three droplets were collected to collect all bubbles of all diameters generated during one period ($\tau = 10$ s) which is in most cases longer than the generation of one droplet. Then, an identical second microscope glass slide was carefully placed on the first one to squeeze the spherical bubble to a cylindrical shape. For more details, we refer to our previous study, ref. [54]. Then one or more microscope pictures (at 5× magnifications) were made with a resolution of 1024 × 1080. Due to the fact that the camera made black-and-white pictures, the emulsion appears dark, whereas the bubbles appears white.

The mean bubble diameters of 100 bubbles were determined by measuring the bubble areas in the original 2D micrographs using ImageJ initially. The bubble areas composing of a large bright area (due to light reflections), being the inner bubble area, and a not directly visible thin dark shell, being the outer bubble area, were determined within the 2D microscope picture(s) (at 5× magnification) using ImageJ. In case of monodisperse foamed emulsions, the inner bubble area (the large bright areas) of the bubbles were automatically determined within the original microscope picture (s), whereas the outer bubble areas were manually determined by encircling the outer dark shell after brightening and contrast (if applicable)

the microscope picture. To calculate the total bubble areas without investing too much effort, we corrected each inner bubble area with a correction value. The correction value is the arithmetic mean of the difference of the outer (manually determined) and inner (automatically determined) area of 20 bubbles. In case of polydisperse foamed emulsions, the total bubble diameter was only manually determined by encircling each outer bubble area. The further quantitative characterization of the foamed emulsions were carried out as described in our previous study, ref. [54]. For the calibration, only pressure settings leading to foamed emulsion monolayers with uniform bubbles having a PDI of $\leq$5% (i.e., monodisperse refs. [59,60]) were considered. Pressure settings which lead to optically nonuniform bubbles (although the PDI was $\leq$5%) or whose diameters change drastically over time were neglected. The software SigmaPlot was used to plot the bubble size distributions with n the number of bubbles normalized to n_{total} (100) the total number of bubbles in a defined diameter range against the bubble diameter. ImageJ was used to add scale bars on all plain micrographs.

SEM and Determination of Pore and Window Diameters: The poly(1,4-BDDMA) foams were characterized using SEM. The samples were frozen in liquid nitrogen and broken or cut with a razor blade into small specimens preferentially horizontally and vertically which was not always possible due to the fragile character of the polymer foams. The specimens were glued on SEM specimen stubs using a conductive silver glue from Plano (Acheson 1415) followed by the whole coating of the sample (excepting its surface) with carbon (from Plano) using the sputter coater Emitech K550. The characterization of each polymer foam was carried out with a TESCAN VEGA3 SEM using second electron imaging (SEI) and a voltage of 5 kV. The corresponding software VegaTC was used to take SEM pictures with a resolution of 1024 × 768.

The polymer foams were quantitatively characterized as described in ref. [54] using the original 2D SEM pictures (at 100× magnification) and taking 100 pores and 25 windows into account. The SEM picture of the Finestructure (Figure 4) was taken at 2000× magnification. The pore size distributions were plotted as described in Section Optical Microscopy and Determination of Bubble Diameters. Beyond the addition of scale bars (see Section Calibration), ImageJ was also used to improve contrast and brightness of all SEM pictures.

Mechanical Properties: The samples of the polymer foams and of the bulk polymers have a cylindrical shape. All samples were synthesized three times. The polymer foams and the bulk polymers were used to determine the relative densities, the porosities, and the mechanical strength. The procedure for the polymer foams was the same as for the bulk polymers. The densities, porosities, and Young's moduli of the polymer foams and the bulk polymers are the averages of the three samples. The density ρ was determined by weighing each polymer foam/bulk polymer and dividing their mass m by their volume as given in

$$\rho = \frac{m}{V} \tag{2}$$

The relative density of the polymer foam was determined by dividing the polymer foam's density ρ_{foam} by the mean bulk polymer density $\rho_{polymer}$. The porosity P of polymer foams was determined as[65]

$$P = (1 - \rho_{foam}) \times 100 \tag{3}$$

The relative densities and porosities of all monodisperse and all polydisperse poly(1,4-BDDMA) foams were averaged. Mechanical compression tests were carried out using the universal testing machine zwickiLine 5 kN from Zwick/Roell equipped with a 5 kN force transducer and regulated by the software testXpert III. Stress–strain curves were measured using normal forces and a testing speed of $1\,mm\,min^{-1}$. The Young's modulus was determined using the slope of a linear part on the beginning of the stress–strain curve corresponding to

$$E = \frac{\sigma}{\varepsilon} = \frac{Fl}{A\Delta l} \tag{4}$$

with σ being the stress defined as the force F acting on a cross-sectional area A and ε being the strain defined as the difference Δl between the sample's height before compression l_0 and after compression l.[64] The Young's modulus of each polymer foam E_{foam} was then normalized by the mean Young's modulus of the bulk polymer E_{bulk}. The Young's moduli of all monodisperse and all polydisperse poly(1,4-BDDMA) foams were averaged.

Conflict of Interest

The authors declare no conflict of interest.

[1] K. Ashida, K. Iwasaki, *Handbook of Plastic Foams, Types, Properties, Manufacture and Applications* (Ed.: A. H. Landrock), Noyes Publications, Park Ridge, NJ, **1995**, pp. 11–220.

[2] M. S. Silverstein, *Prog. Polym. Sci.* **2014**, *39*, 199.

[3] S. Andrieux, W. Drenckhan, C. Stubenrauch, *Langmuir* **2018**, *34*, 1581.

[4] S. Andrieux, A. Quell, C. Stubenrauch, W. Drenckhan, *Adv. Colloid Interface Sci.* **2018**, *256*, 276.

[5] C. Stubenrauch, A. Menner, A. Bismarck, W. Drenckhan, *Angew. Chem. Int. Ed.* **2018**, *57*, 10024.

[6] J. M. Williams, D. A. Wrobleski, *Langmuir* **1988**, *4*, 656.

[7] J. M. Williams, A. J. Gray, M. H. Wilkerson, *Langmuir* **1990**, *6*, 437.

[8] J. M. Williams, *Langmuir* **1991**, *7*, 1370.

[9] P. Hainey, I. M. Huxham, B. Rowatt, D. C. Sherrington, *Macromolecules* **1991**, *24*, 117.

[10] N. R. Cameron, D. C. Sherrington, L. Albiston, D. P. Gregory, *Colloid Polym. Sci.* **1996**, *274*, 592.

[11] N. R. Cameron, *Polymer* **2005**, *46*, 1439.

[12] A. Menner, R. Powell, A. Bismarck, *Soft Matter* **2006**, *2*, 337.

[13] T. Gitli, M. S. Silverstein, *Soft Matter* **2008**, *4*, 2475.

[14] A. Quell, J. Elsing, W. Drenckhan, C. Stubenrauch, *Adv. Eng. Mater.* **2015**, *17*, 604.

[15] A. Quell, B. de Bergolis, W. Drenckhan, C. Stubenrauch, *Macromolecules* **2016**, *49*, 5059.

[16] A. Quell, T. Sottmann, C. Stubenrauch, *Langmuir* **2017**, *33*, 537.

[17] A. Quell, S. Heitkam, W. Drenckhan, C. Stubenrauch, *Chem. Phys. Chem.* **2017**, *18*, 451.

[18] R. Moglia, M. Whitely, M. Brooks, J. Robinson, M. Pishko, E. Cosgriff-Hernandez, *Macromol. Rapid Commun.* **2014**, *35*, 1301.

[19] R. S. Moglia, M. Whitely, P. Dhavalikar, J. Robinson, H. Pearce, M. Brooks, M. Stuebben, N. Cordner, E. Cosgriff-Hernandez, *Biomacromolecules* **2014**, *15*, 2870.

[20] E. M. Christenson, W. Soofi, J. L. Holm, N. R. Cameron, A. G. Mikos, *Biomacromolecules* **2007**, *8*, 3806.

[21] R. S. Moglia, J. L. Holm, N. A. Sears, C. J. Wilson, D. M. Harrison, E. Cosgriff-Hernandez, *Biomacromolecules* **2011**, *12*, 3621.

[22] J. L. Robinson, R. S. Moglia, M. C. Stuebben, M. A. P. McEnery, E. Cosgriff-Hernandez, *Tissue Eng. A* **2014**, *20*,1103.

[23] J. L. Robinson, M. A. P. McEnery, H. Pearce, M. E. Whitely, D. J. Munoz-Pinto, M. S. Hahn, H. Li, N. A. Sears, E. Cosgriff-Hernandez, *Tissue Eng. A* **2016**, *22*, 403.

[24] M. E. Whitely, J. L. Robinson, M. C. Stuebben, H. A. Pearce, M. A. P. McEnery, E. Cosgriff-Hernandez, *ACS Biomater. Sci. Eng.* **2017**, *3*, 409.

[25] N. Sears, P. Dhavalikar, M. Whitely, E. Cosgriff-Hernandez, *Biofabrication* **2017**, *9*, 025020.

[26] M. L. Dabrowski, D. Jenkins, E. Cosgriff-Hernandez, C. Stubenrauch, *Phys. Chem. Chem. Phys.* **2020**, *22*, 155.

[27] P. Krajnc, D. Štefanec, I. Pulko, *Macromol. Rapid Commun.* **2005**, *26*, 1289.

[28] A. Barbetta, M. Dentini, M. S. De Vecchis, P. Filippini, G. Formisano, S. Caiazza, *Adv. Funct. Mater.* **2005**, *15*, 118.

[29] A. Barbetta, M. Dentini, E. M. Zannoni, M. E. De Stefano, *Langmuir* **2005**, *21*, 12333.

[30] A. Barbetta, M. Massimi, B. Di Rosario, S. Nardecchia, M. De Colli, L. Conti Devirgiliis, M. Dentini, *Biomacromolecules* **2008**, *9*, 2844.

[31] S. Kovačič, D. Štefanec, P. Krajnc, *Macromolecules* **2007**, *40*, 8056.

[32] A. Barbetta, E. Barigelli, M. Dentini, *Biomacromolecules* **2009**, *10*, 2328.

[33] S. Vílchez, L. A. Pérez-Carrillo, J. Miras, C. Solans, J. Esquena, *Langmuir* **2012**, *28*, 7614.

[34] J. Miras, S. Vílchez, C. Solans, J. Esquena, *J. Colloid Interface Sci.* **2013**, *410*, 33.

[35] J. Miras, S. Vílchez, C. Solans, T. Tadrosb, J. Esquena, *Soft Matter* **2013**, *9*, 8678.

[36] M. Costantini, C. Colosi, J. Guzowski, A. Barbetta, J. Jaroszewicz, W. Święszkowski, M. Dentini, P. Garstecki, *J. Mater. Chem. B* **2014**, *2*, 2290.

[37] A. Barbetta, A. Gumiero, R. Pecci, R. Bedini, M. Dentini, *Biomacromolecules* **2009**, *10*, 3188.

[38] J.-y. Lin, W.-j. Lin, W.-h. Hong, W.-c. Hung, S. H. Nowotarski, S. Montenegro Gouveia, I. Cristo, K.-H. Lin, *Soft Matter* **2011**, *7*, 10010.

[39] C. Colosi, M. Costantini, A. Barbetta, R. Pecci, R. Bedini, M. Dentini, *Langmuir* **2013**, *29*, 82.

[40] K.-y. Chung, N. C. Mishra, C.-c. Wang, F.-h. Lin, K.-h. Lin, *Biomicrofluidics* **2009**, *3*, 022403.

[41] A. Barbetta, A. Carrino, M. Costantini, M. Dentini, *Soft Matter* **2010**, *6*, 5213.

[42] M. Costantini, C. Colosi, J. Jaroszewicz, A. Tosato, W. Święszkowski, M. Dentini, P. Garstecki, A. Barbetta, *ACS Appl. Mater. Interfaces* **2015**, *7*, 23660.

[43] M. Costantini, C. Colosi, P. Mozetic, J. Jaroszewicz, A. Tosato, A. Rainer, M. Trombetta, W. Święszkowski, M. Dentini, A. Barbetta, *Mater. Sci. Eng. C* **2016**, *62*, 668.

[44] A. Testouri, C. Honorez, A. Barillec, D. Langevin, W. Drenckhan, *Macromolecules* **2010**, *43*, 6166.

[45] S. Andrieux, W. Drenckhan, C. Stubenrauch, *Polymer* **2017**, *126*, 425.

[46] S. Andrieux, L. Medina, M. Herbst, L. A. Berglund, C. Stubenrauch, *Composites A* **2019**, *125*, 105516.

[47] F. Dehli, L. Riebers, A. Southan, C. Stubenrauch, *Biomacromolecules* **2019**, *20*, 2666.

[48] C. Claaßen, M. Claaßen, V. Truffault, L. Sewald, G. E. M. Tovar, K. Borchers, A. Southan, *Biomacromolecules* **2018**, *19*, 42.

[49] L. Sewald, C. Claaßen, T. Götz, M. H. Claaßen, V. Truffault, G. E. M. Tovar, A. Southan, K. Borchers, *Macromol. Biosci.* **2018**, *18*, 1800168.

[50] F. Schüler, D. Schamel, A. Salonen, W. Drenckhan, M. D. Gilchrist, C. Stubenrauch, *Angew. Chem. Int. Ed.* **2012**, *51*, 2213.

[51] J. Elsing, PhD Thesis, Universität Stuttgar 2016t, Shaker-Verlag, Aachen, **2017**, ISBN 978-3-8440-5264-0.

[52] J. Elsing, T. Stefanov, M. D. Gilchrist, C. Stubenrauch, *Phys. Chem. Chem. Phys.* **2017**, *19*, 5477.

[53] J. Elsing, A. Quell, C. Stubenrauch, *Adv. Eng. Mater.* **2017**, *19*, 1700195.

[54] M. L. Dabrowski, M. Hamann, C. Stubenrauch, *RSC Adv.* **2020**, *10*, 8917.

[55] A. Salonen, R. Lhermerout, E. Rio, D. Langevina, A. Saint-Jalmes, *Soft Matter* **2012**, *8*, 699.

[56] S. Yang, K.-F. Leong, Z. Du, C.-K. Chua, *Tissue Eng.* **2001**, *7*, 679.

[57] P. X. Ma, *Mater. Today* **2004**, *7*, 30.

[58] F. J. O´Brien, *Mater. Today* **2011**, *14*, 88.

[59] W. Drenckhan, D. Langevin, *Curr. Opin. Colloid Interface Sci* **2010**, *15*, 341.

[60] A. Maestro, W. Drenckhan, E. Rio, R. Höhler, *Soft Matter* **2013**, *9*, 2531.

[61] H. M. Princen, *Langmuir* **1988**, *4*, 164.

[62] L. J. Gibson, *J. Biomech.* **2005**, *38*, 377.

[63] M. Ashby, R. M. Medalist, *Metall. Trans. A* **1983**, *14A*, 1755.

[64] L. J. Gibson, M. F. Ashby, *Cellular Solids, Structures and Properties*, Cambridge University Press, Cambridge **1999**.

[65] N. Mills, *Polymer Foams Handbook*, Elsevier, Oxford **2007**.

[66] Dolomite, Droplet Junction Chips, Product Datasheet, file:///C:/Users/N7D18~1.DAB/AppData/Local/Temp/Dolomite_DropletJunctionChipDatasheet_pdf.pdf, (accessed: July 2020).

2001013 (12 of 12)